Available online at www.sciencedirect.com

ScienceDirect

Publishing Services by Elsevier

International Journal of Naval Architecture and Ocean Engineering 10 (2018) 259–269
http://www.journals.elsevier.com/international-journal-of-naval-architecture-and-ocean-engineering/

Prediction of the wave induced second order vertical bending moment due to the variation of the ship side angle by using the quadratic strip theory

Seunglyong Kim, Jungsoo Ryue*, In-Kyu Park

School of Naval Architecture and Ocean Engineering, University of Ulsan, South Korea

Received 28 November 2016; revised 15 May 2017; accepted 12 July 2017
Available online 14 August 2017

Abstract

In this study, the second order bending moment induced by sea waves is calculated using the quadratic strip theory. The theory has the fluid forcing terms including the quadratic terms of the hydrodynamic forces and the Froude–Krylov forces. They are applied to a ship as the external forces in order to estimate the second order ship responses by fluid forces. The sensitivity of the second order bending moment is investigated by implementing the quadratic terms by varying the ship side angle for two example ships. As a result, it was found that the second order bending moment changes significantly by the variation of the ship side angle. It implies that increased flare angles at the bow and the stern of ships being enlarged would amplify their vertical bending moments considerably due to the quadratic terms and may make them vulnerable to the fatigue.

Keywords: Springing; Quadratic strip theory; The second order vertical bending moment; Froude-Krylov force; Hydrodynamic force

1. Introduction

Recently, merchant ships become larger but relatively lighter than before, in terms of the non-dimensionalized displacement, to reduce the transportation costs. In case of container ships recently constructed, for instance, their sizes are capable of carrying more than 20000 TEU and growing continuously. By being larger and lighter, their natural frequencies tend to move down to lower frequencies. Therefore, they are likely to experience resonant vibration, so called springing, more easily in service. This is because their natural frequencies become closer to the excitation frequencies of incoming waves.

The ship's resonant vibration can be induced by the quadratic components of sea waves as well as the first order ones (Tasai and Koterayama, 1976). The amplitude of the response at the resonance produced by the second order components of the sea waves is generally known to be much smaller when compared to that by the first order ones. However in case of ships in severe conditions such as in the Arctic Ocean, the second order resonant vibration could cause significant fatigue problems, because it is proportional to the square of the wave amplitude (Fujino and Yoon., 1985). This situation makes fatigue loads being increased, and consequently shortens the life of ships. Therefore, in terms of the long term response analysis, the accurate estimation of the second order responses should be included, regarding a significant resonant steady-state response. In terms of the fatigue loads, the vertical bending moment would be the primary component. So, in this study the vertical bending moment at midship is of interest.

As ships are enlarged, their bow and stern are flared much because their breadths increase more than their drafts. This shape trend would make the second order vertical bending moment increase due to risen wave loads at the bow and stern. Thus it would be necessary to understand the characteristics of the vertical bending moment for the variation of ship side angle, including the second order components. The ship side

* Corresponding author.
E-mail address: jsryue@ulsan.ac.kr (J. Ryue).
Peer review under responsibility of Society of Naval Architects of Korea.

http://dx.doi.org/10.1016/j.ijnaoe.2017.07.002

angle is defined as an angle of a ship side inclined from a vertical line. This study aims to investigate the contribution of the second order terms on the ship's vertical bending moments. The variation of the second order term is introduced by the change of the ship's side angle. In order to make only the second order terms vary, the ship side is allowed to be inclined within slightly above and below the mean water level.

In this study, two ships are chosen; one is an artificial ship with a uniform cross-section and the other is a Flokstra container ship as a practical one. The ships are assumed as Timoshenko beams with free-ends (Bishop and Price, 1979). Fluid forces are applied to the ships as external forces to calculate their responses induced by sea waves. The second order terms of the fluid forces are calculated using the quadratic strip theory that is proposed by Jensen and Pedersen (1979). The second order vertical bending waves are predicted at midship by varying the ship side angle.

2. Theoretical background

In this section, theoretical models used in this study to predict the ship response is explained, regarding the second order terms induced by wave loads. External fluid forces are formulated using a quadratic strip theory, proposed by Jensen and Pedersen (1979), which includes second order terms for the fluid forces (Xia et al., 1998). The second order fluid forces are taken into account by three quadratic parameters. The first parameter is the second order velocity potential for the incident wave, which is obtained from the non-linear free boundary conditions. The second one is associated with a non-vertical side of ship cross-sections, which occurs when the breadth of a ship varies along with the depth about waterline. This variation of the breadth also makes a non-linearity of a restoring force. The last one is a quadratic hydrodynamic coefficient; the variation of the added mass and the damping. Both are dependent on the relative motion between the ship and the wave surface. As a result, the second order hydrodynamic and the Froude–Krylov forces are applied as the external forces in addition to the first order ones.

The structural response of a ship is formulated using a Timoshenko beam theory. The response of the ship is predicted by applying the hydrodynamic and Froude–Krylov force.

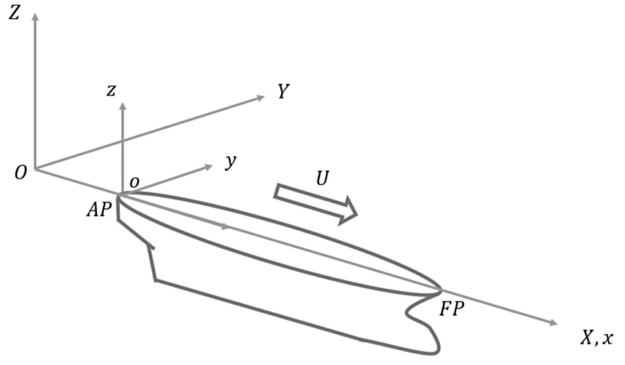

Fig. 1. The coordinate system.

In this study two Cartesian coordinate systems are adopted as shown in Fig. 1. The global coordinate *OXYZ* is fixed with an origin in still water level while the local coordinate *oxyz* is attached on the ship with the origin at the stern of the ship. These two coordinates coincide when the ship is at rest. The ship is assumed to have a forward speed U toward the positive X direction, corresponding to a heading angle of 180°, called the 'head sea'.

2.1. Quadratic strip theory for fluid force

The fluid force per unit length applied on a ship is formulated using a quadratic strip theory that considers the change of added mass, damping and restoring terms depending on the relative motion between the ship and the wave surface. For a ship with a sectional breadth $B(z,x)$ and draft $T(x)$, this fluid force per unit length is given by

$$F(x,t) = -\left[\frac{D}{Dt}\left\{m(\bar{z},x)\frac{D\bar{z}}{Dt}\right\} + N(\bar{z},x)\frac{D\bar{z}}{Dt} + \int_{-T}^{-\bar{z}} B(z,x)\frac{\partial p}{\partial Z}\bigg|_{z+w} dz\right], \tag{1}$$

where $\frac{D}{Dt}$ denotes the total derivative with respect to time as $\frac{D}{Dt} = \frac{\partial}{\partial t} - U\frac{\partial}{\partial x}$, $w(x,t)$ is the vertical displacement of the ship and $\bar{z}$ is the relative displacement of $\bar{z} = w - \kappa h$, $\kappa(x)$ is the Smith correction factor, $h(x, t)$ is the wave elevation, $m(\bar{z}, x)$ and $N(\bar{z}, x)$ denote the added mass per unit length and the damping at the water surface respectively, and $p(x, Z, t)$ is the Froude–Krylov pressure. Eq. (1) has the same form as the linear strip theory which contains only the linear terms of the fluid forces (Gerritsma and Beukelman, 1964). In order to take into account the second order terms of the fluid forces, Taylor series expansion is applied to the added mass m, the damping N and the breadth B with respect to the relative motion $\bar{z}(x,t)$ at a mean water level. Applying Taylor series about $\bar{z}$,

$$m(\bar{z},x) = m(0,x) + \bar{z}\frac{\partial m}{\partial \bar{z}}\bigg|_{\bar{z}=0} + \frac{1}{2}\bar{z}^2\frac{\partial^2 m}{\partial \bar{z}^2}\bigg|_{\bar{z}=0} + \ldots \cong m(0,x) + \bar{z}\frac{\partial m}{\partial \bar{z}}\bigg|_{\bar{z}=0} = m_0(x) + \bar{z}m_1(x), \tag{2}$$

$$N(\bar{z},x) = N(0,x) + \bar{z}\frac{\partial N}{\partial \bar{z}}\bigg|_{\bar{z}=0} + \frac{1}{2}\bar{z}^2\frac{\partial^2 N}{\partial \bar{z}^2}\bigg|_{\bar{z}=0} + \ldots \cong N(0,x) + \bar{z}\frac{\partial N}{\partial \bar{z}}\bigg|_{\bar{z}=0} = N_0(x) + \bar{z}N_1(x), \tag{3}$$

$$B(\bar{z},x) = B(0,x) + \bar{z}\frac{\partial B}{\partial \bar{z}}\bigg|_{\bar{z}=0} + \frac{1}{2}\bar{z}^2\frac{\partial^2 B}{\partial \bar{z}^2}\bigg|_{\bar{z}=0} + \ldots \cong B(0,x) + \bar{z}\frac{\partial B}{\partial \bar{z}}\bigg|_{\bar{z}=0} = B_0(x) + \bar{z}B_1(x), \tag{4}$$

where $B(\overline{z},x)$ is the breadth of the ship with respect to the relative displacement, and the subscripts 0 and 1 represent the constant and linear terms with respect to $\overline{z}$ at waterline, respectively. In this approximation in Eqs. (2)–(4), only the constant and linear terms are regarded because they become the respective linear and quadratic terms about $\overline{z}$ when they are substituted into Eq. (1).

The added mass and the damping are evaluated by Porter's method (Porter, 1961) and Tasai's method (Tasai, 1960) in this study. They transform a cross-sectional shape of a ship into a two parameter Lewis form in order to describe the added mass and the damping as simple functions of with respect to breadth, draft and cross-sectional area (Vugts, 1968). Because they have different frequency ranges applicable, Porter's method is used for encounter frequencies below 1 ($\omega_e < 1$) and Tasai's for encounter frequencies above 1 ($\omega_e \geq 1$) in this study (Heo et al., 2016).

2.2. Restoring forces

The Froude–Krylov force, so called undisturbed incident wave force, is expressed by

$$F_R(x,t) = -\int_{-T}^{-\overline{z}} B(z,x)\frac{\partial p}{\partial Z}\Big|_{z+w} dz. \tag{5}$$

In Eq. (5), the pressure p is based on the Bernoulli's equation and given by

$$p(x,Z,t) = \rho\left\{\frac{\partial\phi}{\partial t} + gZ + \frac{1}{2}(\nabla\phi)^2\right\}, \tag{6}$$

where $\phi(x, Z, t)$ is the wave velocity potential, g is the gravitational acceleration, ρ is the water density and ∇ denotes the gradient. Eq. (6) can be expanded by a perturbation method as

$$p = p^{(0)} + p^{(1)} + p^{(2)} + \ldots, \tag{7}$$

where

$$p^{(0)} = -\rho g Z, \tag{8}$$

$$p^{(1)} = -\rho\frac{\partial\phi^{(1)}}{\partial t}, \tag{9}$$

$$p^{(2)} = -\rho\left\{\frac{\partial\phi^{(2)}}{\partial t} + \frac{1}{2}\left(\nabla\phi^{(1)}\right)^2\right\}. \tag{10}$$

$p^{(0)}(Z)$ is the static component of the restoring force and $p^{(1)}(x, Z, t)$ and $p^{(2)}(x, Z, t)$ are the dynamic force components that are proportional to the wave amplitude and the square of the wave amplitude, respectively. In Eqs. (9) and (10), $\phi^{(1)}$ and $\phi^{(2)}$ are the first and second order terms of the wave velocity potentials, respectively. These terms are obtained by introducing the non-linear boundary conditions to the first and second order wave elevation $h^{(1)}(x, t)$ and $h^{(2)}(x, t)$, given by Eqs. (12) and (13).

$$h = h^{(1)} + h^{(2)} + \ldots, \tag{11}$$

where

$$h^{(1)}(x,t) = \sum_{i=1}^{n} a_i\cos(\psi_i), \tag{12}$$

$$h^{(2)}(x,t) = \frac{1}{4}\sum_{i=1}^{n}\sum_{j=1}^{n} a_i a_j\left[\left(k_i + k_j\right)\cos\left(\psi_i + \psi_j\right) - \left|k_i - k_j\right|\cos\left(\psi_i - \psi_j\right)\right]. \tag{13}$$

In Eqs. (12) and (13), a_i is the amplitude of the i th wave, and n is the number of waves considered. The phase angle ψ_i of the i th wave is defined by

$$\psi_i = -k_i X - \sigma_i t + \theta_i, \tag{14}$$

where k_i is the wavenumber, θ_i is the initial phase angle and σ_i is the angular wave frequency obtained from the dispersion relation of the sea wave, given by $\sigma_i = \sqrt{gk_i}$. In Eq. (14), the horizontal position X can be expressed by the coordinate x as $x = X - Ut$.

The first and the second order velocity potentials of the incident waves (Longuet-Higgins, 1963) are expressed as

$$\phi^{(1)}(x,Z,t) = \sum_{i=1}^{n}\frac{a_i\sigma_i}{k_i}e^{k_i Z}\sin(\psi_i), \tag{15}$$

$$\phi^{(2)}(x,Z,t) = \frac{1}{2}\sum_{i=1}^{n}\sum_{j=1}^{n} a_i a_j\max\left(-\sigma_i,\sigma_j\right)e^{\left|k_i-k_j\right|Z}\sin\left(\psi_i - \psi_j\right), \tag{16}$$

where

$$\max\left(-\sigma_i,\sigma_j\right) = \begin{cases} -\sigma_i & if\ \ \sigma_i \geq \sigma_j \\ \sigma_j & if\ \ \sigma_i < \sigma_j \end{cases}.$$

By inserting Eqs. (15) and (16) into Eqs. (9) and (10), the expanded expressions of the pressures are described by

$$p^{(1)}(x,Z,t) = \rho g\sum_{i=1}^{n} a_i e^{k_i Z}\cos(\psi_i), \tag{17}$$

$$p^{(2)}(x,Z,t) = -\frac{1}{2}\rho\sum_{i=1}^{n}\sum_{j=1}^{n} a_i a_j\Big\{\max\left(\sigma_i,\sigma_j\right)\left|\sigma_i - \sigma_j\right|e^{\left|k_i-k_j\right|Z} + \sigma_i\sigma_j e^{\left(k_i+k_j\right)Z}\Big\}\cos\left(\psi_i - \psi_j\right). \tag{18}$$

Substituting Eqs. (17) and (18) into Eq. (7), the wave induced restoring force in Eq. (5) is described with the linear and quadratic terms as shown in Eqs. (19)–(21).

$$F_R(x,t) = F_R^{(1)} + F_R^{(2)}, \tag{19}$$

where

$$F_R^{(1)}(x,t) = -\rho g B_0 \left\{ w_1 - \sum_{r=1}^{n} a_r \kappa_r \cos(\psi_r) \right\}, \tag{20}$$

$$\begin{aligned} F_R^{(2)}(x,t) = {} & -\rho g B_0 w_2 + \frac{1}{2}\rho g B_0 w_1^2 - \rho g w_1 \sum_{i=1}^{n} a_i \cos(\psi_i)(B_1 \\ & - B_0 k_i \kappa_i) + \frac{1}{4}\rho g \sum_{i,j=1}^{n} a_i a_j \{\cos(\psi_i + \psi_j) B_1 \\ & + \cos(\psi_i - \psi_j) \times [B_1 + 2B_0 \{ (\sqrt{k_i k_j} \\ & - \max(k_i k_j)) \kappa_{|i-j|} - \sqrt{k_i k_j}\, \kappa_{i+j} \}] \}. \end{aligned} \tag{21}$$

In Eqs. (20) and (21), w_1 and w_2 are the first and second order vertical displacements of the ship. The Smith correction factor κ_i and $\kappa_{|i\pm j|}$ is expressed by

$$\begin{aligned} \kappa_i(x) &= 1 - \frac{k_i}{B_0(x)} \int_{-T}^{0} B(z,x)^{k_i z} dz, \\ \kappa_{|i+j|}(x) &= 1 - \frac{|k_i \pm k_j|}{B_0(x)} \int_{-T}^{0} B(z,x) e^{|k_i \pm k_j| z} dz. \end{aligned} \tag{22}$$

2.3. Hydrodynamic force

The hydrodynamic force per unit length $F_H(x,t)$ is composed of the inertia force and damping force terms expressed by

$$F_H(x,t) = -\frac{D}{Dt}\left(m \frac{D\bar{z}}{Dt} \right) - N \frac{D\bar{z}}{Dt}. \tag{23}$$

This hydrodynamic force can be expanded by using the approximations in Eqs. (2) and (3) and also for the relative displacement $\bar{z} \cong \bar{z}_1 + \bar{z}_2$, respectively. Then the hydrodynamic force with the linear and quadratic terms can be expressed by

$$F_H = F_H^{(1)} + F_H^{(2)}, \tag{24}$$

where

$$F_H^{(1)}(x,t) = -m_0 \frac{D^2 \bar{z}_1}{Dt^2} - n_0 \frac{D\bar{z}_1}{Dt}, \tag{25}$$

$$\begin{aligned} F_H^{(2)}(x,t) = {} & -m_0 \frac{D^2 \bar{z}_2}{Dt^2} - n_0 \frac{D\bar{z}_2}{Dt} - \bar{z}_1 \left(m_1 \frac{D^2 \bar{z}_1}{Dt^2} + n_1 \frac{D\bar{z}_1}{Dt} \right) \\ & - m_1 \left(\frac{D\bar{z}_1}{Dt} \right)^2, \end{aligned} \tag{26}$$

Here, $\bar{z}_1$ and $\bar{z}_2$ are the first and second order terms of the relative displacement and n_o and n_1 are defined by

$$n_0(x) = N_o - U \frac{\partial m_0}{\partial x}, \tag{27}$$

$$n_0(x) = N_o - U \frac{\partial m_0}{\partial x}, \tag{28}$$

The relative displacements $\bar{z}$ can be substituted with terms of the first and second order wave heights $h^{(1)}$, $h^{(2)}$, the Smith correction factor κ and the vertical displacement w of the ship. Then the hydrodynamic forces are expressed by

$$\begin{aligned} F_H^{(1)}(x,t) = {} & -m_0 \frac{D^2 w_1}{Dt^2} - n_0 \frac{Dw_1}{Dt} - \sum_{i=1}^{n} a_i \sigma_i \kappa_i \{ m_0 \sigma_i \cos(\psi_i) \\ & - n_0 \sin(\psi_i) \}, \end{aligned} \tag{29}$$

$$\begin{aligned} F_H^{(2)}(x,t) = {} & -m_0 \frac{D^2 w_2}{Dt^2} - n_0 \frac{Dw_2}{Dt} - w_1 \left(m_1 \frac{D^2 w_1}{Dt^2} + n_1 \frac{Dw_1}{Dt} \right) \\ & - m_1 \left(\frac{Dw_1}{Dt} \right)^2 + \sum_{i=1}^{n} a_i \kappa_i \left\{ \cos(\psi_i) \left[m_1 \frac{D^2 w_1}{Dt^2} \right. \right. \\ & \left. + n_1 \frac{Dw_1}{Dt} - \sigma_i^2 m_1 w_1 \right] + \sin(\psi_i) \left[n_1 \sigma_i w_1 \right. \\ & \left. \left. + 2 m_1 \sigma_i \frac{Dw_1}{Dt} \right] \right\} + \frac{1}{4} \sum_{i=1}^{n} \\ & \times \sum_{j=1}^{n} a_i \kappa_i a_j \kappa_j \left\{ \cos(\psi_i + \psi_j) (\sigma_i + \sigma_j)^2 (m_1 \right. \\ & - (k_i + k_j) m_0) + \cos(\psi_i - \psi_j) (\sigma_i - \sigma_j)^2 (m_1 \\ & + |k_i - k_j| m_0) + \sin(\psi_i + \psi_j) (\sigma_i + \sigma_j) (-n_1 \\ & + (k_i + k_j) n_0) + \sin(\psi_i - \psi_j) (\sigma_i - \sigma_j) (-n_1 \\ & \left. - |k_i - k_j| n_0). \right. \end{aligned} \tag{30}$$

2.4. Equation of motion for a ship using a Timoshenko beam theory

The equation of motion for a ship can be derived as a Timoshenko beam with free−free boundary conditions. The constituent equations of the Timoshenko beam are given by

$$M(x,t) = EI \frac{\partial \gamma}{\partial x} + \eta EI \frac{\partial^2 \gamma}{\partial x \partial t}, \tag{31}$$

$$V(x,t) = KAG \left(\frac{\partial w}{\partial x} - \gamma \right) + \eta KAG \left(\frac{\partial^2 w}{\partial x \partial t} - \frac{\partial \gamma}{\partial t} \right), \tag{32}$$

where $M(x, t)$ is the vertical bending moment, $V(x, t)$ is the shear force, γ denotes the angle of rotation, η is the structural damping, E and G are Young's and shear moduli, I is the area moment of inertia and A is the sectional area, K is the shear coefficient of the cross section. Applying the equilibrium conditions for the moment and shear force,

$$\frac{\partial M(x,t)}{\partial x} = -V(x,t) + I_{\mu x} \frac{\partial^2 \gamma}{\partial t^2}, \tag{33}$$

$$\frac{\partial V(x,t)}{\partial x} = \mu(x) \frac{\partial^2 w}{\partial t^2} - F(x,t), \tag{34}$$

where $I_{\mu x}$ is the mass moment of inertia, $\mu(x)$ is the mass per unit length and $F(x, t)$ is the external fluid force. By substituting Eqs. (31) and (32) into Eqs. (33) and (34), the equations of motion are given by

$$\frac{\partial}{\partial x}\left[EI\left(1+\eta\frac{\partial}{\partial t}\right)\frac{\partial \gamma}{\partial x}\right]+KGA\left(1+\eta\frac{\partial}{\partial t}\right)\left(\frac{\partial w}{\partial x}-\gamma\right) = I_{\mu x}(x)\frac{\partial^2\gamma}{\partial t^2}, \tag{35}$$

$$\frac{\partial}{\partial x}\left[KGA\left(1+\eta\frac{\partial}{\partial t}\right)\left(\frac{\partial w}{\partial x}-\gamma\right)\right] = \mu(x)\frac{\partial^2 w}{\partial t^2}-F(x,t). \tag{36}$$

Here, the eigenvalue problem of the beam is solved by applying the free–free boundary conditions at both ends of the beam in order to obtain the natural frequencies and the mode shapes for the vertical directional motion. The vertical displacement and the rotational angle are expressed by the modal superposition as

$$\gamma(x,t)=\sum_{i=0}^{N}u_i(t)\alpha_i(x) \tag{37}$$

$$w(x,t)=\sum_{i=0}^{N}u_i(t)v_i(x) \tag{38}$$

where α_i and v_i denote the i–th mode shapes (Cuthill and Henderson, 1925) for the rotational angle and vertical displacement, respectively, and u_i is the time dependent modal amplitude. The subscript, $i = 0$, 1 and 2 represent the heave, pitch and two node vibration modes, respectively. By inserting Eqs. (37) and (38) into Eqs. (35) and (36), and applying the orthogonality relations between each mode, the governing equation in the modal domain is written by

$$\ddot{u_j}+\eta\Omega_j^2\dot{u_j}+\Omega_j^2u_j=\int_0^L v_jF\left(x,t,\sum_{i=0}^{N}u_iv_i\right)dx. \tag{39}$$

Here, Ω_j is the j–th natural frequency of the beam. Since the quadratic terms were included in the derivation of Eq. (39), u_j is also expressed as a sum of the linear and quadratic terms as

$$u_j=u_j^{(1)}+u_j^{(2)}. \tag{40}$$

Using the terms of the mode shapes and Eq. (40), the first and second order vertical displacements and rotational angles are obtained from Eqs. (37) and (38). Then finally the first and second order vertical bending moments and shear forces in Eqs. (31) and (32) can be calculated, respectively (Betts et al., 1974).

3. Numerical simulations for artificial ships

In the previous section, the equations for the ship response caused by regular waves were formulated by including the quadratic components. In order to examine the contribution of the quadratic terms to the ship response in this section, the calculation of the second order vertical bending moment is carried out by changing the ship side angle artificially. This simulation is carried out choosing two ship models, which are an ideal ship with a uniform cross-section and Flokstra container ship (Flokstra, 1974) as a practical one.

3.1. Example 1. A ship with a uniform cross-section

To observe the variation of the second order vertical bending moment induced by incoming waves, a uniform ship that has a constant cross-section along its length as shown in Fig. 2 is investigated in this example. The principal dimensions of the uniform ship are listed in Table 1.

In Fig. 2, $\Delta\bar{z}$ denotes the variable range of the draft of the ship, and θ is the ship angle of the side varying. B_u and B_l denote the breadths at $\Delta\bar{z}$ above and below the waterline, respectively. In this simulation, it is desired that the linear terms in the quadratic strip theory are little influenced by the variation of θ in order to see only the perturbation of the quadratic terms. To achieve this purpose, the ship side angle θ is assumed to be changed only within slightly above and below the waterline. So several different values of $\Delta\bar{z}$ were examined and finally $\Delta\bar{z}$ was chosen to be 0.1 m in this example. The rate of change of the breadth against the relative displacement $\bar{z}$ can be defined by the ship side angle as

$$B_1=\left.\frac{\partial B}{\partial\bar{z}}\right|_{\bar{z}=0}=\frac{B_u-B_l}{2\Delta\bar{z}}=2\tan\theta. \tag{41}$$

The prediction is conducted inclining θ from 0 to 70° with a 10° interval. The limit of 70° is chosen based on the stern side angles of practical container ships.

Above all, the first order bending moments M_1 at the midship section of the uniform ship are illustrated in Fig. 3 for various side angles. Fig. 3 shows that the first order bending moment has two dominant peaks: the first one at around 0.8 rad/s is correspond to the hogging and sagging motions of the ship, which occurs when the wave length matches with the ship length. The highest peak at around 3.12 rad/s, called 'the

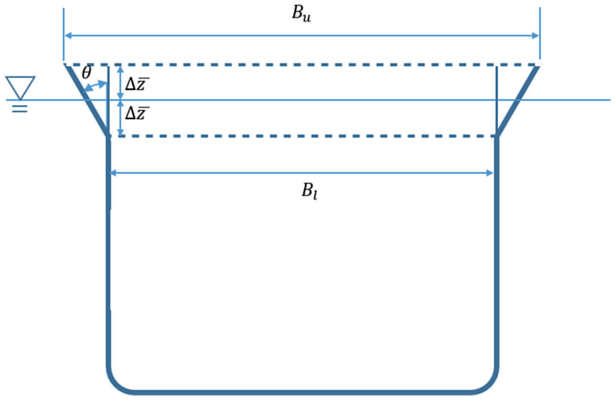

Fig. 2. Body plan of a ship with a uniform cross-section.

Table 1
Principal dimensions of the uniform ship.

LBP (m)	270
Breadth (m)	31.9
Draft (m)	10.26
Structural damping factor	0.001

second peak' hereafter in this paper, takes place due to the two node resonant vibration of the ship. It can be seen from Fig. 3 that the first order bending moment does not affected by the side angle variation as intended. It means that the variation of the ship side angle has little effect on the added mass and damping because the ship side angle was restricted to vary only around the waterline in this analysis.

There are two values of the second order vertical bending moments, which are called M_{20} and M_{22} in general. M_{20} is a response caused by a second order wave component having a frequency difference of $\sigma_i - \sigma_j$. It implies 'mean drift' of the second order vertical bending moment. M_{22} is induced by a second order wave component, so called 'sum frequency' which has the sum of two frequencies $\sigma_i + \sigma_j$. Non-dimensional M_{20} is illustrated in Fig. 4 and it grows as the ship side angle increases at the hogging and sagging frequency. It implies that the ship side angle increases the mean drift of the second order bending moment increase due to the difference between the hogging and sagging motion. The variation of non-dimensional M_{22} for the uniform ship induced

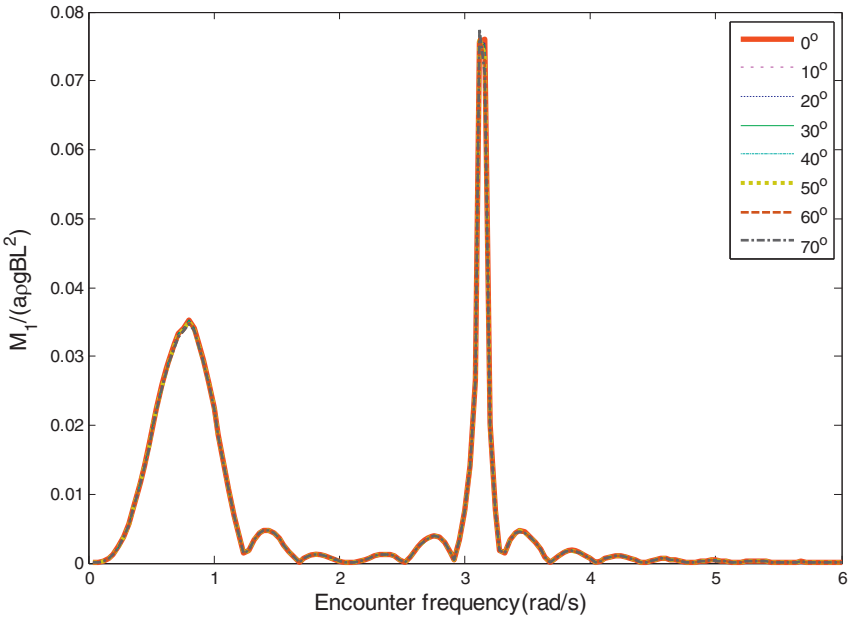

Fig. 3. Non-dimensional first order vertical bending moments of the uniform ship.

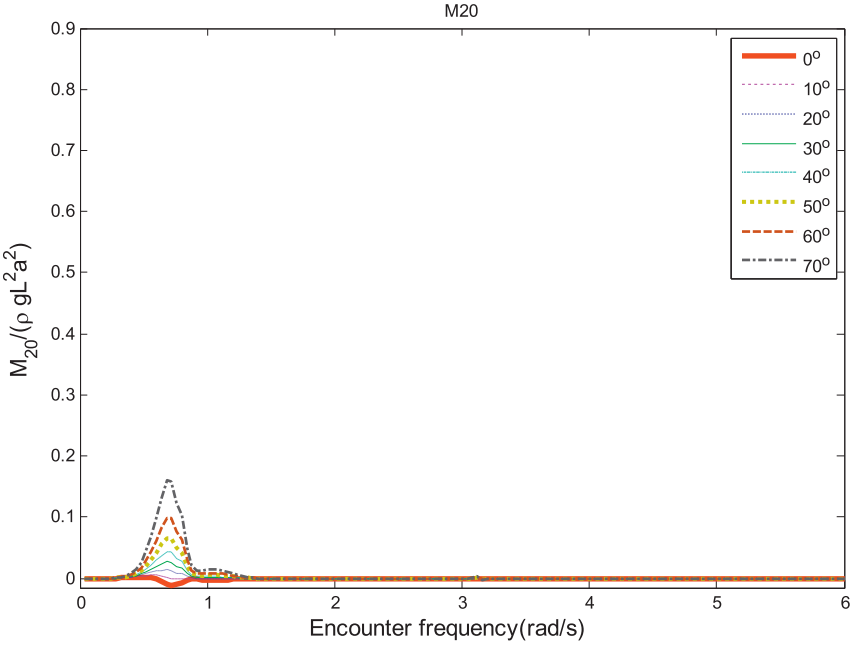

Fig. 4. Non-dimensional M_{20} of the uniform ship.

by the sum frequency wave is shown in Fig. 5. Unlike the first order one in Fig. 3, it can be seen from Fig. 5, the ship side angle contributes strongly to M_{22}. M_{22} drops first and then grows as the side angle increases at the two peak frequencies. Here the first peak at 0.8 rad/s represents the moment at the hogging and sagging frequency, and the second peak at 1.56 rad/s corresponds to the two node resonant frequency. It can be seen that the frequency of the two node resonance in Fig. 5 is a half of the first order one shown in Fig. 3 because the wave frequency is doubled when the two frequencies σ_i and σ_j are the same.

In this study, it is more interested in examining M_{22}, rather than M_{20}, so that the variation of M_{22} is investigated further at the two peak frequencies. In order to look close the variation of M_{22} at the two peaks in Fig. 5, M_{22} at 0.8 and 1.56 rad/s are plotted again in Fig. 6 against the ship side angle. It can be seen from Fig. 6 that the amplitudes of M_{22} at the two peak frequencies decrease as the ship side begins to incline, but turn to grow as the angle goes further, particularly at the second peak.

This feature can be explained by regarding at the variation of the fluid forcing terms against the side angle. The inertia,

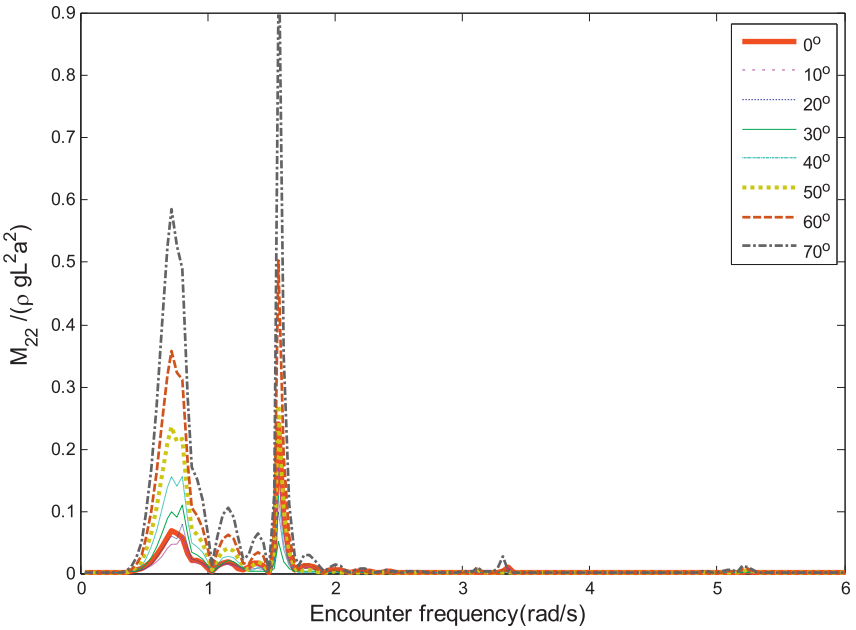

Fig. 5. Non-dimensional M_{22} of the uniform ship.

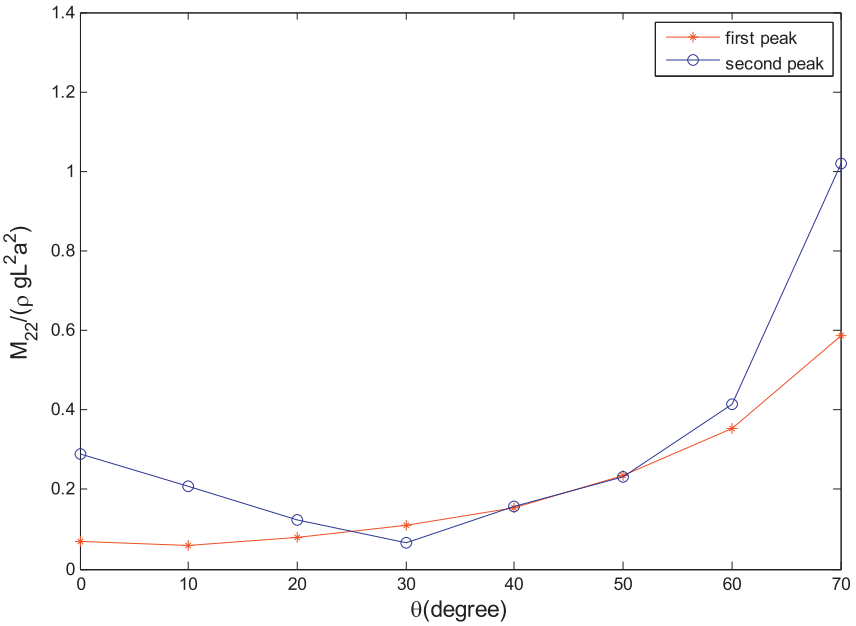

Fig. 6. The peak values versus the uniform ship side angle.

damping and restoring fluid forces in Eqs. (21) and (30) can be rewritten by

$$B(\bar{z},x)-\omega^2 m_z(\bar{z},x)=B(0,x)+\bar{z}\frac{\partial B}{\partial \bar{z}}\bigg|_{\bar{z}=0}-\omega^2\left[m_z(0,x)+\bar{z}\frac{\partial m_z}{\partial \bar{z}}\bigg|_{\bar{z}=0}\right]=B(0,x)-\omega^2 m_z(0,x)+\bar{z}\left[B_1-\omega^2 m_{z_1}\right], \tag{42}$$

where $m_z = m - Ni/\omega$, $m_{z1} = \partial m/\partial \bar{z} - (i/\omega)\partial N/\partial \bar{z}$ and i denotes the imaginary number.

In Eq. (42), the inertia force and the restoring force are applied in opposite directions. At $\theta = 0°$, B_1 in Eq. (42) becomes zero because the breadth remains constant along the depth direction at this angle. Therefore, the second order net force $\bar{z}(B_1 - \omega^2 m_{z1})$ becomes equal to the inertia force. As the ship side angle inclines, both B_1 and m_{z1} increase but B_1 will grow faster than m_{z1} because the variation of the breadth is limited just around the waterline. Fig. 7 shows the magnitude of the second order net forces at two peak frequencies calculated by Eqs. (21) and (30). The amplitude of force at 1.56 rad/s is decreasing until θ reaches to an angle that the inertia force and the restoring force are canceled out, which is around 30° where the vertical bending moment has minimum value. After the restoring force exceeds the inertia force, the second order net force increases exponentially with θ. At 0.8 rad/s, on the other hand, the force is just increasing in Fig. 7, because the term $\omega^2 m_{z1}$ is negligible at this frequency. It is sure from the comparison between the results in Figs. 6 and 7 that variation of the forces at the two peak frequencies in Fig. 7 resembles that of M_{22} in Fig. 6. It also can be seen from Fig. 6 that the peak values increase more rapidly with the large angles. This implies that the second order bending moment becomes more sensitive to the largely inclined ship sides. From this result, therefore, it is anticipated that the inclined sides at the bow and stern in practical ships would cause significant effect on the second order vertical bending moment of the ships.

3.2. Example 2. Flokstra container ship

In order to evaluate the variation of the second order response of a practical ship due to the inclined ship sides, a Flokstra container ship is chosen in this section. Fig. 8 illustrates the body plan of the Flokstra container ship and the principal dimensions are listed in Table 2. The ship side angles at each station are set to be varied with fixed rates of ±2, ±4 and ±6% with respect to the given initial angles around the waterline shown in Fig. 8. Since the angle varies with rates to the initial inclination, the side angles at the stern and bow

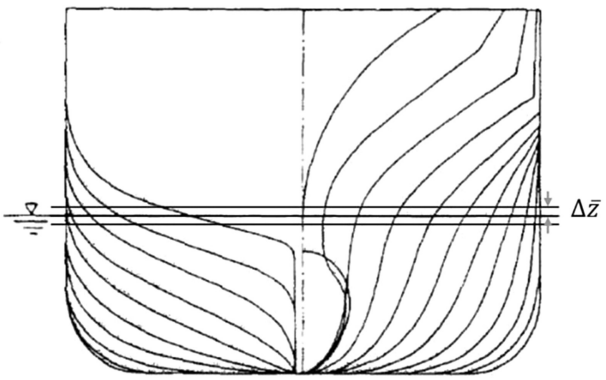

Fig. 8. The body plan of Flokstra container ship (Flokstra, 1974).

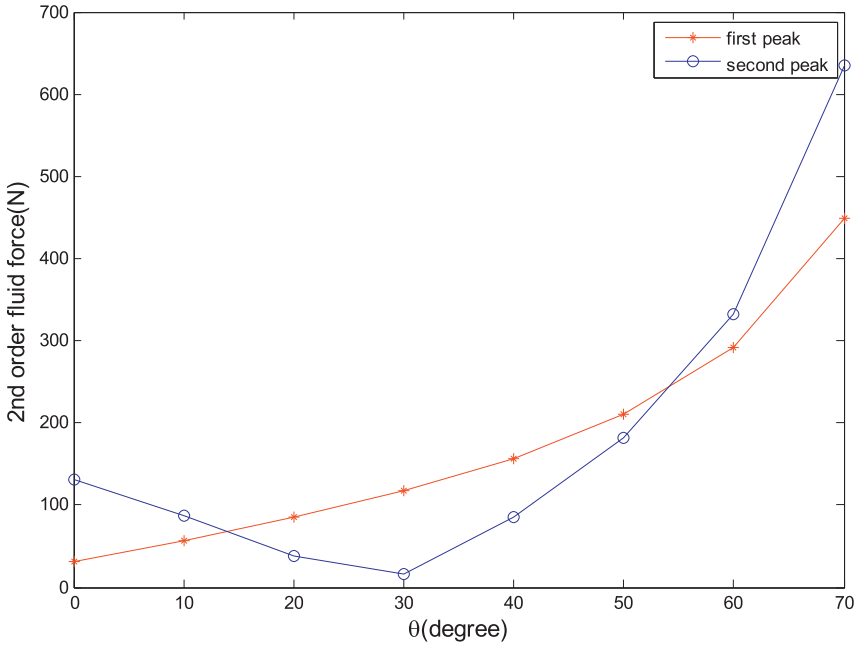

Fig. 7. The external force versus with respect to the ship side angle.

Table 2
Principal dimensions of the Flokstra container ship.

LBP (m)	270
Breadth (m)	32.2
Draft (m)	10.26
Structural damping factor	0.001

varies more widely compare to the stations close to the midship. The largest change of the side angle occurs at the stern section for about 1.5° with the rate of 2% variation of the side angle. In case of the midship, the side angle is not changed by these rates because its initial angle is 0°. These variations of the side angle are assumed to take place only within a draft range between 0.1 m below and above the waterline as regarded in Example 1 for the uniform ship.

The first order vertical bending moments M_{11} at the midship section are shown in Fig. 9 for various side angles. They are little changed by the side angle variations as observed in the uniform section ship. However, in case of M_{22} illustrated in Fig. 10, the change of the ship side angle makes a large perturbation, particularly around the second peak at 2.2 rad/s, which corresponds to the two node resonant frequency of the ship. Therefore, it can be said from Fig. 10 that the inclination of the ship side, especially at the stern and bow sections,

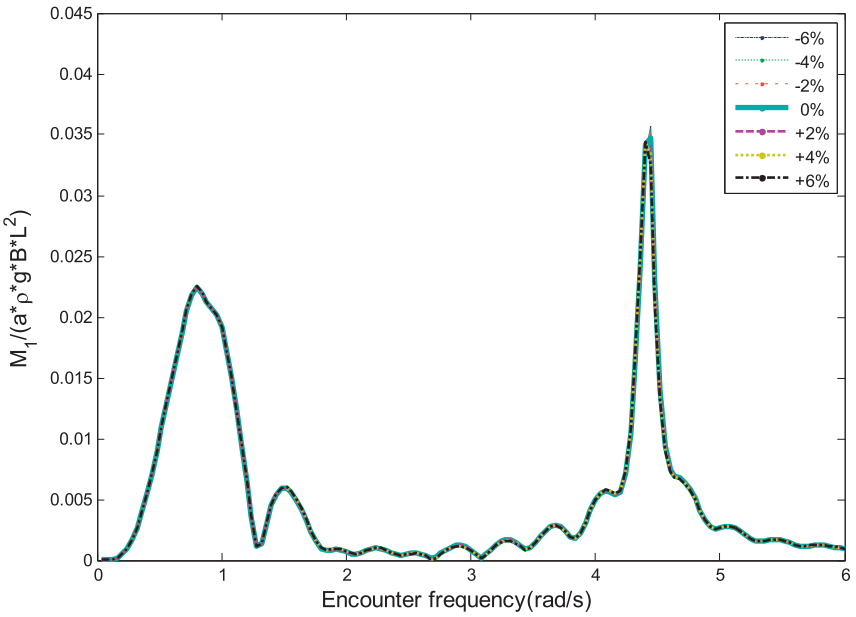

Fig. 9. Non-dimensional first order bending moments of the Flokstra ship.

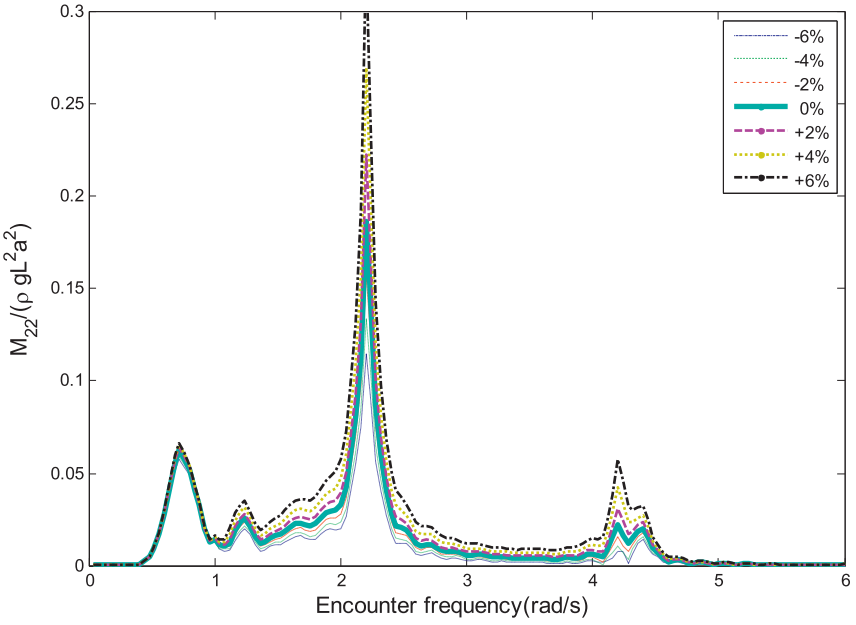

Fig. 10. Non-dimensional second order vertical bending moments of the Flokstra ship.

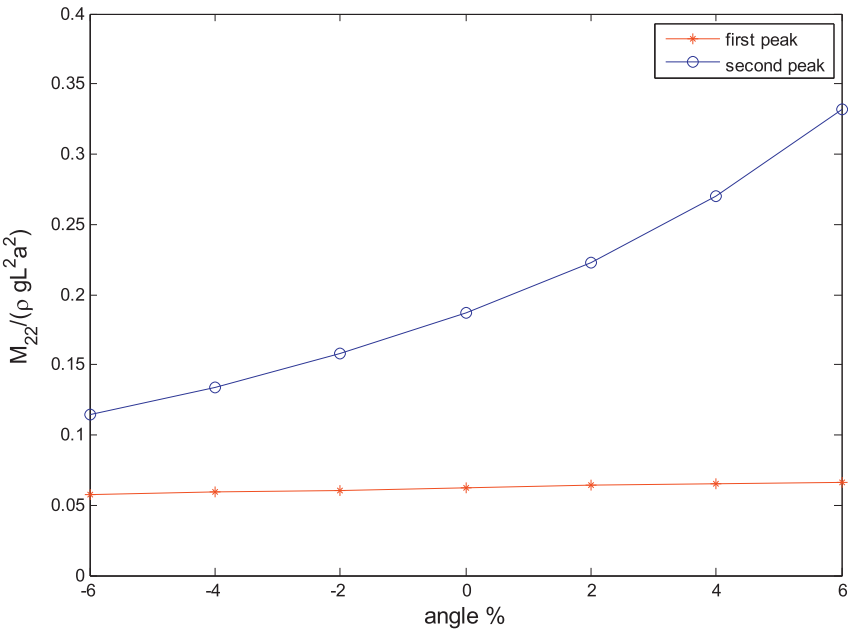

Fig. 11. The peak values changing with respect to the Flokstra ship side angle.

makes a considerable variation of the second order bending moment of the ship.

The variation of M_{22} of the Flokstra ship at the first peak at 0.72 rad/s and second peaks are plotted in Fig. 11 with respect to the inclined rate. Dislike those from the uniform ship, they increases monotonically as the angle increases. It is because that the side angles at the stern and bow of the Flokstra ship are large enough so that the restoring force is always bigger than the inertia force from the beginning. For example, the initial side angle of the stern section is about 73°, so that the second order vertical bending moment has a large increment following the tendency of the result in Fig. 6.

4. Conclusions

In this paper, the responses of ships induced by wave loads were investigated by using the quadratic strip theory. To do that, the linear and quadratic terms of fluid forces were involved in modeling wave loads while ships were supposed as a Timoshenko beam with free–free boundaries. The fluid forces were applied to the ships as external forces which are induced by incoming sea waves.

In this study, it was attempted to examine the contribution of the quadratic terms to the vertical bending moment of ships. For this purpose, the quadratic terms were introduced to the fluid forces by changing the breadth of ships artificially. Two ship models were chosen; one is a uniform ship with a constant cross-section along its length and the other is a Flokstra container ship. For these two ships the side angles were set to be varied just around the waterline to keep the linear terms maintained and then the perturbation of the second order vertical bending moment were predicted.

It is confirmed from this study that the vertical bending moment varies significantly due to the quadratic terms. In case of the uniform ship model, the second order bending moment tends to decrease and then increase with the ship side angle variation due to the relation between the inertia and restoring forces in opposite directions. The quadratic term of the inertia force, which is dependent on the cross sectional area, has maintained nearly the same despite of the ship side angles, while that of the restoring force has increased rapidly as the ship side angle increases. That is, the variation of the ship side angle could increase the quadratic buoyancy force term, so the total force become increasing after the buoyancy force is over the inertia force.

In addition, it was found that the second order bending moment becomes more sensitive for larger side angles. In case of a Flokstra ship which has large side angles at the stern and bow, it can be expected that the stern and bow sides govern the second order bending moments. In this case the second order vertical bending moment just increased as the ship side angle increases. This feature comes from a condition that the bow and stern sections have large initial inclinations from the beginning. That is, they were large enough to make the second order initial buoyance force become greater than that of inertia force. Therefore the second order terms of the external force is increasing as the ship side angle increases.

This study has limited to regular incident waves at head sea. In the future, this study needs to be conducted for the irregular wave cases. Also short term and long term statistics will be required to be carried out in order to investigate the characteristics of the fatigue stress for the ship side angle change.

References

Betts, C.V., Bishop, R.E.D., Price, W.G., 1974. The symmetric generalised fluid forces applied to a ship in a seaway. Trans. RINA 119.

Bishop, R.E.D., Price, W.G., 1979. Hydro-Elasticity of Ships. Cambridge University Press.

Cuthill, E.H., Henderson, F.M., 1925. Description and Usage of General Bending Response Code 1 (GBRC1).

Flokstra, C., 1974. Comparison of ship motion theories with experiments for a containership. Int. Shipbuild. Prog. 21, 168–189.

Fujino, M., Yoon, B.S., 1985. A study on wave loads acting on a ship in large amplitude waves. J. Soc. Nav. Archit. Jpn. 157, 155–167.

Gerritsma, J., Beukelman, W., 1964. The distribution of the hydrodynamic forces on a heaving and pitching ship model in still water. In: Fifth Symposium on Naval Hydrodynamics, pp. 219–251.

Heo, K.-U., Koo, W., Park, I.-K., Ryue, J., 2016. Quadratic strip theory for high-order dynamic behavior of a large container ship with 3D flow effects. Int. J. Nav. Archit. Ocean Eng. 8 (2), 127–136.

Jensen, J.J., Pedersen, P.T., 1979. Wave induced bending moments in ships – a quadratic theory. In: R. Inst. Nav. Archit. Supplementary Papers, pp. 151–166.

Longuet-Higgins, M.S., 1963. The effect of non-linearities on statistical distributions in the theory of sea waves. J. Fluid Mech. 17 (3), 459–480.

Porter, W.R., 1961. Pressure Distributions, Added-mass and Damping Coefficients for Cylinders Oscillating in a Free Surface. University of California at Berkeley (Doctoral Thesis).

Tasai, F., 1960. On the Damping Force and Added Mass of Ships Heaving and Pitching. University of California at Berkeley Institute of Engineering Research.

Tasai, F., Koterayama, W., 1976. Nonlinear hydrodynamic forces acting on cylinders heaving on the surface of a fluid. Report of research institute for applied mechanics. Kyushu Univ. 12 (77), 1–39.

Vugts, J.H., 1968. The Hydrodynamic Coefficients for Swaying, Heaving and Rolling Cylinders in a Free Surface. Report No. 194.

Xia, J., Wang, Z., Jensen, J.J., 1998. Non-linear wave loads and ship responses by a time-domain strip theory. Mar. Struct. 11, 101–123.